

Article

Maintenance and Restoration Effect of the Surface Hydrophilicity of Pure Titanium by Sodium Hydroxide Treatment and Its Effect on the Bioactivity of Osteoblasts

Lulu Jiang ¹, Shan Jin ², Shuangshuang Geng ¹, Chunfu Deng ¹, Zeng Lin ³ and Baohong Zhao ^{1,*}

¹ Center of Implant Dentistry, School of Stomatology, China Medical University, Shenyang 110002, China; lljiang@cmu.edu.cn (L.J.); jhe@cmu.edu.cn (S.G.); cfdeng@cmu.edu.cn (C.D.)

² Department of Oromaxillofacial-Head and Neck Surgery, Department of Oral and Maxillofacial Surgery, School of Stomatology, China Medical University, Shenyang 110002, China; jinshan@cmu.edu.cn

³ School of Mechanical Engineering & Automation, Northeastern University, Shenyang 110004, China; zlin@mail.neu.edu.cn

* Correspondence: bhzhao@cmu.edu.cn; Tel.: +86-24-3192-7731

Received: 27 February 2019; Accepted: 24 March 2019; Published: 28 March 2019



Abstract: In recent years, studies on the surface of titanium implants have shown that hydrophilic properties have a positive effect on bone binding, warranting further investigation into the maintenance and restoration of hydrophilic properties. In this work, a hydrophilic surface was obtained by plasma oxidation on the surface of sandblasted and acid-etched (SLA) titanium discs. We aimed to determine the effect of sodium hydroxide (NaOH) treatment on the maintenance and restoration of the surface hydrophilicity of titanium discs, as well as the relationship between the changes in hydrophilic properties on titanium surfaces and their biological properties. The results show that the treatment of hydrophilic surfaces with SLA, plasma oxidation, and NaOH treatments tend to enhance the early stages of cell adhesion, proliferation, and differentiation. Those results provide important guidance that SLA, plasma oxidation, and NaOH treatments can be used to restore the hydrophilic property of Ti that has been stored under room temperature and atmospheric pressure conditions.

Keywords: dental implant; hydrophilicity; surface modification; sodium hydroxide; osseointegration

1. Introduction

Compared with fixed partial dentures or removable dentures, implant-supported prostheses provide comfort and good esthetics and have therefore earned a favorable reputation from both patients and dentists [1]. Good biocompatibility, ideal soft and hard tissue integration, adequate mechanical strength, and physiologic transmission of masticatory forces to bone are necessary to achieve good functionality for dental implants [2]. One of the critical elements that influences the long-term functioning of dental implants is osseointegration. However, the bone–implant contact percentage has remained around 45%–65% [3,4]. Therefore, improvement of the osseointegration rate is increasingly being pursued by dentists. In recent years, clinicians have been more eager to get early osseointegration after implantation in order to shorten the repair time and reduce the risk of failure.

A series of papers indicated that the generation and maintenance of bone around an implant are closely related to the biological activity of the dental implant surfaces, which is determined by the physical and chemical properties. From the perspective of tissue engineering, implant surface microstructure appears to work as a scaffold for osseointegration [5,6]. Optimization of the scaffold plays a pivotal role in determining how many osteogenic cells are attracted to the local environment

with preferable expressions of the necessary biological signals, eventually leading to an improved peri-scaffold bone formation [7]. Titanium and titanium alloys are generally accepted and applied in terms of dental implant materials. In recent years, some scholars have suggested that titanium could be replaced with polyetheretherketone (PEEK) as a dental implant material. However, unmodified PEEK is less osseointegrative and bioactive than titanium [8]. However, Ti and Ti alloys are inert materials that cannot be chemically bonded with bone tissue. Therefore, many subtractive and additive techniques have been introduced to alter the surface morphology of implants, such as sandblasting, acid etching, oxidizing, or combinations of these techniques [9–11]. Sandblasting and acid etching (SLA) is one of the most commonly used methods.

In general, wettability on micro-structured surfaces decreases when generated by sandblasting, acid etching, or oxidizing [12]. The presence of micro-and/or nanostructures, as found on newly developed surface modifications, might also modulate hydrophilicity and the corresponding biological response [13]. Att and Hori confirmed that the protein adsorption capacity, osteoblast adhesion, proliferation, differentiation, and the osseointegration ability decreased with a prolonged preservation time [14,15]. Studies have shown that the decrease in bioactivity may be due to contamination by hydrocarbons. Kilpadi and Serro corroborated that hydrocarbons in the air, water, or cleaning fluid can be continuously adsorbed onto the surface of the material so that the Ti discs are likely to have a significant decrease in hydrophilic properties during storage [16,17]. Lu also showed that hydrocarbon contamination reduces the hydrophilicity of Ti discs, which is not conducive to the adhesion and proliferation of osteoblasts [18].

In clinical applications, the implants have likely been stored for a certain period of time, and the hydrophilicity of the implant surface could have been reduced, thereby leading to altered biological properties. Stefano Tugulu et al. [19] stored titanium discs with superhydrophilic surfaces in alkali solution and found that the contact angle of the titanium surface was greatly reduced after alkali treatment, indicating that alkali treatment could maintain the hydrophilicity of the titanium surface. Studies have shown that the –OH group is the main reason for the hydrophilicity of TiO_x thin films [20]. The process of alkali treatment occurring on the surface of TiO_{2-x} is mainly due to the protonation and dephosphorization of Ti–OH and Ti–O–Ti [21]. The materials used in this study were super hydrophilic Ti discs prepared by plasma oxidation and NaOH. The aim of the present study was to determine the effects of SLA, plasma oxidation, and NaOH treatment on the restoration and maintenance of the hydrophilicity of the Ti discs, which is critical to allow clinical implants to achieve proper osseointegration.

2. Materials and Methods

2.1. Preparation of Ti Samples

Disc-shaped Ti samples (10 and 15 mm in diameter, 1.5 mm in thickness) were prepared from commercially pure grade-4 titanium (provided by the College of Machinery and Automation, Northeast University, Shenyang, China). The Ti discs were ultrasonically cleaned with acetone, anhydrous ethanol, and dH_2O for 5 min each. The SLA surface was prepared by sandblasting with TiO_2 (large grits of 0.25–0.50 mm) followed by acid etching at 100 °C for 20 min. The mixed acid contained 60% H_2SO_4 , 10% HCl, and deionized water with a volume ratio of 1:1:2. The NaOH solution had a concentration of 0.1 mol/L. After soaking in 0.1 mol/L NaOH solution, the Ti discs were cleaned with deionized water for 10 s. After sandblasting and acid etching, the samples were subjected to plasma oxidation treatment. Before oxidation, they were cleaned by Ar plasma to remove the impurities adsorbed on the surface of the samples. By using plasma-enhanced chemical vapor deposition (PECVD) equipment (RF-500, Cross-Tech Equipment Co., Ltd., Shanghai, China), the oxygen plasma produced by vacuum glow discharge bombarded the surface of SLA samples, resulting in the generation of super hydrophilic TiO_x thin films. Non-thermal atmospheric pressure plasma (NTAPP) oxidation treatment was carried out at a constant voltage, using a homemade pulse DC power supply with 200 W. The DC bias voltage

was 400 V, and the oxidation time was set in the range of 60 min. The working pressure was 6.5 Pa, and the volume flow ratio of O₂ and Ar was 1 (Ar = 5 sccm). After sample preparation, Ti discs were assigned to 4 groups: (1) control group SLA Ti discs were stored for 10 days at room temperature and atmospheric pressure (SLA group); (2) SLA Ti discs were stored for 10 days at room temperature and atmospheric pressure and were immersed in 0.1 mol/L NaOH solution for 10 s (SLA/NaOH-10s group); (3) SLA Ti discs oxidized by electrolytic plasma were stored for 10 days at room temperature and atmospheric pressure and were immersed in 0.1 mol/L NaOH solution for 10 s (SLA-PECVD/NaOH-10s group); (4) SLA Ti discs oxidized by electrolytic plasma were immersed in 0.1 mol/L NaOH solution for 10 days (SLA-PECVD/NaOH-10d group). In addition, SLA Ti discs oxidized by electrolytic plasma and immersed in 0.1 mol/L NaOH solution for 200 days (SLA-PECVD/NaOH-200d) were prepared for the testing of surface characterization.

2.2. Surface Characterization

The surface morphology of the samples was observed using a scanning electron microscope (SEM; SSX-550, Shimadzu, Kyoto, Japan). The hydrophilicity of the surfaces was evaluated by the contact angle (CA) of 1 µL ddH₂O using an automatic contact angle measurement device (SL200B, Shanghai, China).

The chemical composition of the Ti sample surface was evaluated by X-ray photoelectron spectroscopy (XPS, ESCALAB250, Thermo VG Company, Waltham, MA, USA), and Al K α (1486.6 eV) X-rays were used as the source with the following parameters: 50 eV, 150 W, and a vacuum degree of 6.0×10^{-8} mbar.

The crystalline structures of the coating before and after machining were investigated by X-ray diffraction (XRD, PW304060, PANalytical B.V. Company, Almelo, the Netherlands) with a Cu K α 1 source.

2.3. Osteoblastic Cell Culture

The MC3T3-E1 cell lines derived from rat calvarial osteoblastic cells were provided by the Central Laboratory of the School of Stomatology, China Medical University, Taichung, Taiwan. The cells were cultured in an α -MEM culture medium (Hyclone, UT, USA) containing 10% fetal bovine serum (FBS), 100 U/mL penicillin G, and 100 µg/mL streptomycin at 37 °C in 5% CO₂ and 95% humidity. An inverted microscope (OLYMPUS, C-35AD, Tokyo, Japan) was used to observe the growth condition of the cells. At 80% confluency, cells were detached using 0.25% trypsin-EDTA to prevent contact inhibition. The culture medium was renewed every 72 h.

2.4. Protein Adsorption Assay

Bovine serum albumin (BSA; Genview, Calimesa, CA, USA) and human fibronectin (Fn; Prospec, East Brunswick, NJ, USA) were used as model proteins. A previously established bicinchoninic acid-based colorimetric detection method (BCA, Biotech Department of Ding Guo Changsheng, Beijing, China) was used to detect the protein adsorption efficiency by following the instructions of the kit [22]. Fn and BSA were pipetted and spread on each sample surface of the Ti discs for each group, and incubated for 3, 6, and 24 h at 37 °C under sterile humidity conditions. Any unadhered protein was removed by rinsing three times with PBS. The specimens were stored in the 96-well cell culture plates with 200 µL of sodium dodecyl sulfate (SDS; 1 wt % Genview, USA) and shaken in a rocking bed (WD-9405B, Beijing, China) for 1 h. Then, the solution containing nonadherent proteins was removed and mixed with 200 µL BCA at 37 °C for 30 min [14,23,24]. Then, standard curves were established according to the optical density (OD), which was quantified with a microplate reader (TECAN, Infinite 200, Yamato, Japan) at 562 nm. Then, the protein adsorption rate was acquired by interpolating the protein content from the standard curve.

2.5. Cell Attachment Assay

Three samples from each group were cultured in the 6-well cell culture plates (1 piece/well). A total of 5×10^4 MC3T3-E1 cells were cultured at 37 °C in 5% CO₂ and 95% humidity and detected at each time point (6, 24, and 48 h). Ti discs from the four groups were transferred to new 6-well cell culture plates and fixed in 2.5% buffered glutaraldehyde. Next, the specimens were gradient dehydrated by ethanol, rinsed twice with distilled water, and dried in air. SEM was performed to confirm the absence of cell remnants on the substrates.

2.6. Cell Proliferation Assay

A total of 2×10^4 MC3T3-E1 cells were cultured at 37 °C in 5% CO₂ and 95% humidity and detected at each time point (1, 3, 5, and 7 days). Samples were transferred to a new 24-well cell culture plates and rinsed twice with PBS. Then, cells were fixed in 800 µL culture fluid and 200 µL MTT (Sigma, Deisenhofen, Germany) at 37 °C. The MTT experiment is to measure the viability and number of living cells by dyeing the living cells and measuring the OD value. After 4 h of culture, 1 mL dimethyl sulfoxide (DMSO, Sigma, Germany) was added and the samples were shaken for 10 min under the condition of strict light avoidance. Two hundred microliters of cell suspension was obtained from each group to place into a 96-well plate to detect the absorbance of each pore at a wavelength of 490 nm by the ELISA meter and to determine the vigor of the osteoblasts.

2.7. Cell Differentiation Assay

The alkaline phosphatase (ALP) activity of cultured osteoblasts was examined by a colorimetric assay. A total of 2×10^4 MC3T3-E1 cells were cultured at 37 °C in 5% CO₂ and 95% humidity, and detected at each time point (3, 5, 10, and 15 days). Samples were transferred to new 24-well cell culture plates and rinsed twice with PBS. Then cells were fixed in trypsin (Hyclone, USA) for 3 min and collected with centrifugation. Twenty microliters of Triton X-100 (0.1%) was added, and the supernatant was carefully collected by centrifuging at 4 °C (12,000 rpm, 5 min). Fifty microliters of Buffer A and 50 µL of Buffer B were added (KGI Nanjing Biological Products Company, Nanjing, China) and cultures were incubated at 37 °C for 15 min. Then, a 200 µL cell suspension was obtained from each group and transferred into a 96-well plate, and then absorbance was read at 520 nm with an ELISA meter, and the content of ALP was determined. A BCA protein assay kit was also used to determine the protein adsorption efficiency by following the instructions. Three microliters of cell suspension and 200 µL of BCA solution were fixed and cultured for 30 min at 37 °C. The protein adsorption efficiency was established according to the optical density (OD), which was quantified with a microplate reader at 562 nm. The ALP activity was calculated by the following formula:

$$\text{ALP activity (mg/gprot)} = \frac{\text{OD}(\text{test}) - \text{OD}(\text{blank})}{\text{OD}(\text{standard}) - \text{OD}(\text{blank})} \times \frac{\text{concentration of phenolics} \left(\frac{0.003 \text{ mg}}{\text{mL}} \right)}{\text{protein concentration of sample} \left(\frac{\text{gprot}}{\text{mL}} \right)}. \quad (1)$$

2.8. Cell Morphology and Morphometry

A total of 2×10^4 MC3T3-E1 cells were cultured at 37 °C in 5% CO₂ and 95% humidity and detected at each time point (1, 2, 4, and 24 h). The Ti discs from the four groups were rinsed three times with PBS and fixed in 2.5% buffered glutaraldehyde at 4 °C. Then, samples were treated with 20 µL 0.1% Triton X-100 for 2 min and stained with phalloidin overnight. Fluorescence microscopy (Nikon 80i, Tokyo, Japan) was used to examine cell morphology and cytoskeletal arrangement.

2.9. Statistical Analysis

SPSS 17.0 software was used for all statistical analyses. Based on the results from previous studies [24–27], data from at least three independent experiments were used. Group means and standard deviations were used to calculate each parameter. The results obtained for the four groups

were analyzed using one-way analysis of variance (ANOVA). A p -value of less than 0.05 was considered statistically significant.

3. Results

3.1. Morphology of Ti Surfaces

The low-magnification and high-magnification SEM images for the four samples (SLA, SLA-PECVD, SLA-PECVD/NaOH-10d, and SLA-PECVD/NaOH-200d) showed similar microrough surfaces (Figure 1). The surfaces of these samples showed a typical microtopographic configuration with irregular crater holes with diameters of 10–30 μm and traffic fusion between holes. No morphological changes were found on the SLA-PECVD surfaces compared with the SLA. The SEM images of PECVD, SLA-PECVD/NaOH-10d, and SLA-PECVD/NaOH-200d indicated that NaOH storing did not change the micropore structure on the surfaces of these discs.

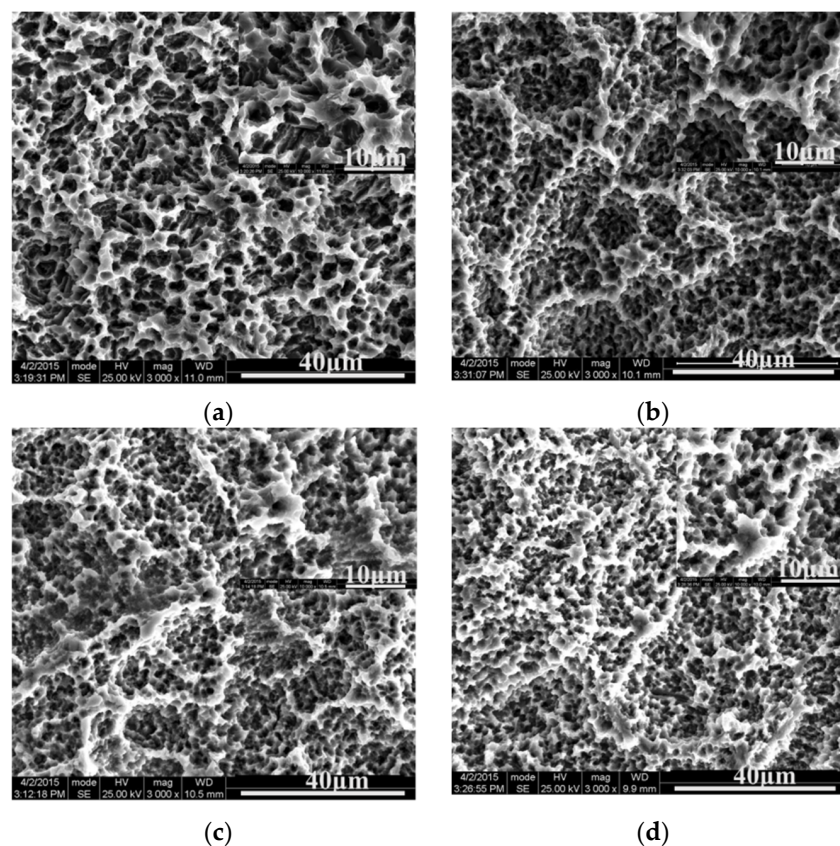


Figure 1. The surface morphologies of the four samples: (a) SLA sample; (b) SLA-PECVD sample; (c) SLA-PECVD/NaOH-10d sample; (d) SLA-PECVD/NaOH-200d sample. No morphological changes were found on the surfaces of the four samples.

XPS provided the elemental compositions of the SLA-PECVD sample and the SLA-PECVD/NaOH-10d sample. The F peak may be caused by some HF acid remaining in the sample during acid etching. The Fe peak may be the impurity component in the matrix material, or its presence may be caused by contamination in the treatment process. In contrast, the surfaces of the lye-stored samples were covered by foreign depositions with clear peaks representing Na (Figure 2). The XPS spectra showed clear peaks of $\text{Ti}2p$, $\text{O}1s$, and $\text{C}1s$ for the two Ti discs' surfaces. In addition to these elements detected on the surfaces, the lye-stored surfaces showed spectra matching the $\text{Na}1s$ (1.50%) listed in Table 1. The $\text{Ti}2p$, $\text{C}1s$, and $\text{O}1s$ XPS spectra of the surfaces of the SLA-PECVD and SLA-PECVD/NaOH-10d samples are shown in Figure 3.

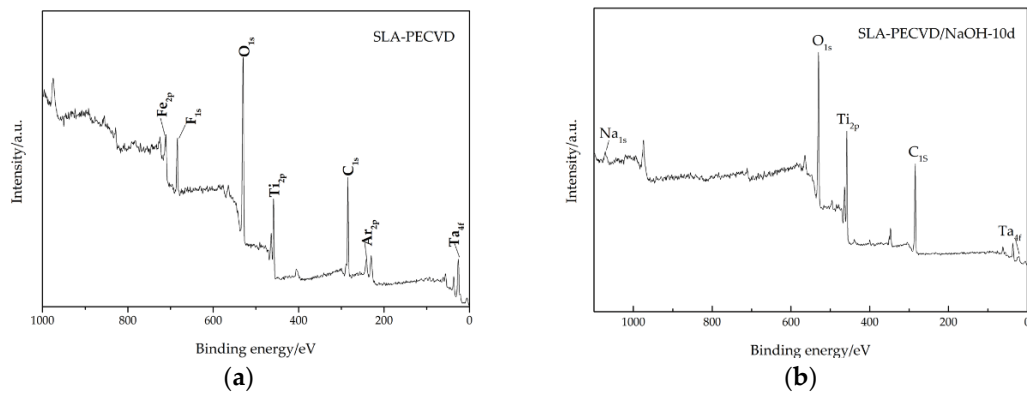


Figure 2. XPS spectrum on the surface of the SLA-PECVD (a) and SLA-PECVD/NaOH-10d (b) samples. The surface of SLA-PECVD/NaOH-10d sample was covered by foreign depositions with clear peaks representing Na.

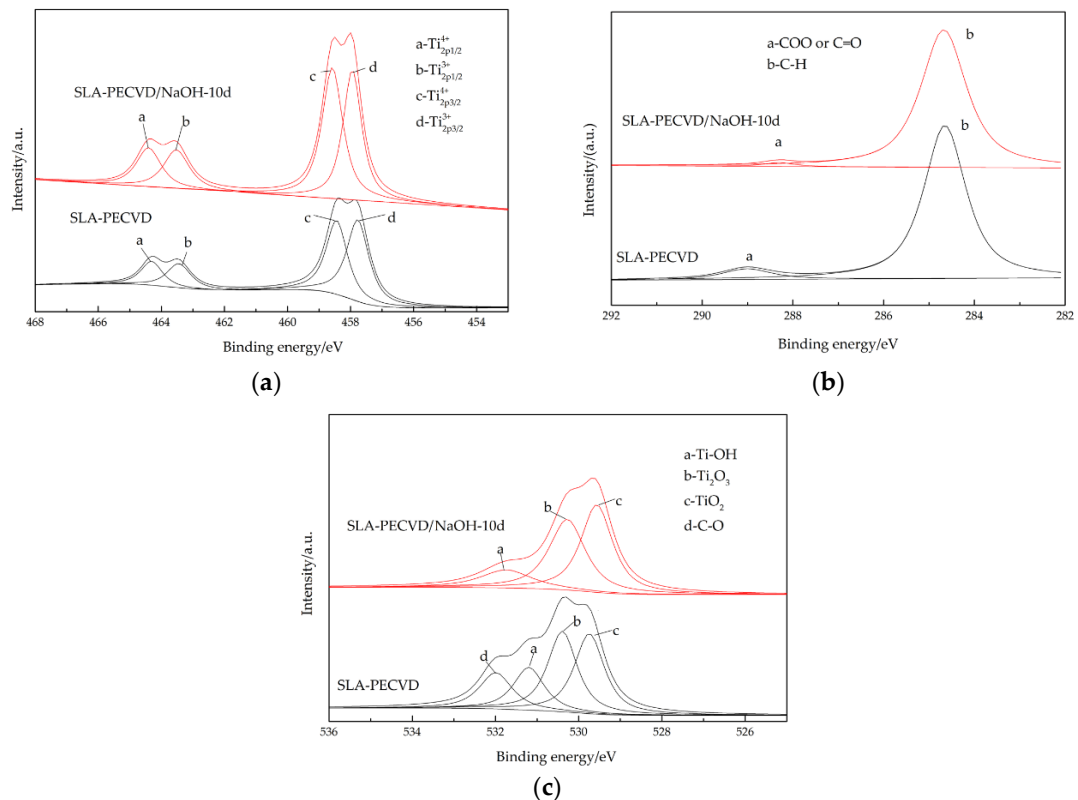


Figure 3. The Ti2p (a), C1s (b), and O1s (c) XPS spectra of the surfaces of the SLA-PECVD and SLA-PECVD/NaOH-10d samples.

Table 1. Elemental composition (at.%) determined by XPS analysis of the SLA-PECVD and SLA-PECVD/NaOH-10d samples.

Ti Discs	Ti	C	O	Na
SLA-PECVD	6.16	43.94	36.41	–
SLA-PECVD/NaOH-10d	10.97	49.23	38.31	1.48

In the SLA-PECVD/NaOH-10d group, the Ti2p XPS spectra were divided into four components with binding energies of 464.4, 458.6, 463.5, and 457.9 eV, which are respectively ascribed to $Ti^{4+}_{2p1/2}$, $Ti^{4+}_{2p3/2}$, $Ti^{3+}_{2p1/2}$, and $Ti^{3+}_{2p3/2}$. There was no change in the valence state, which is the same as the

result of plasma oxidation. However, according to the area of each peak, the proportion of Ti in each valence state was different. As shown in Table 2, the proportion of $Ti^{3+}_{2p3/2}$ on the surface of the SLA-PECVD/NaOH-10d sample decreased by 6% compared with that of SLA-PECVD sample, while the proportions of other valence states increased. The proportions of TiO_2 and Ti_2O_3 were 52.09% and 47.94% in the SLA-PECVD/NaOH-10d sample, and the corresponding ratios for SLA-PECVD were 46.74% and 53.26%, respectively. Therefore, NaOH storage did not change the valence state of Ti discs, mainly in the presence of +4 and +3 valence, but the contents of both changed.

Different from the SLA-PECVD sample, for the SLA-PECVD/NaOH-10d sample, only three O1s spectral peaks were obtained after the Gauss peak fitting treatment. Regarding the O1s peaks, the peaks corresponding to Ti–O (TiO_2), Ti–O (Ti_2O_3), and the hydroxyl group (Ti–OH) had binding energies of 529.6, 530.3, and 531.7 eV, respectively. It can be seen from Table 3 that the oxygen on the surface of SLA-PECVD/NaOH-10d Ti discs mainly existed in the form of TiO_2 and Ti_2O_3 in proportions of 44.42% and 40.77%. The level of Ti–OH dropped immediately after lye storage, from 22.90% to 14.84%. The change in the ratio of the Ti–OH group may have been caused by the higher rate of CA of the sample after NaOH solution treatment.

Table 2. Binding energy, area, and proportion of the $Ti2p$ peaks for the SLA-PECVD and SLA-PECVD/NaOH-10d samples.

Ti Discs		$Ti^{4+}_{2p1/2}$	$Ti^{4+}_{2p3/2}$	$Ti^{3+}_{2p1/2}$	$Ti^{3+}_{2p3/2}$
SLA-PECVD	Eb/eV	464.3	458.4	463.4	457.8
	area	6207.7	18,771.7	6915.8	21,548.0
	r/%	11.62	35.12	12.94	40.32
SLA-PECVD/NaOH-10d	Eb/eV	464.4	458.6	463.5	457.9
	area	11,608.4	32,829.5	11,876.4	29,007.8
	r/%	13.61	38.48	13.92	34.00

Table 3. Binding energy, area, and proportion of the O1s peaks for the SLA-PECVD and SLA-PECVD/NaOH-10d samples.

Ti Discs		Ti–O (TiO_2)	Ti–O (Ti_2O_3)	Ti–OH	C–O
SLA-PECVD	Eb/eV	529.8	530.5	531.2	532.0
	area	46,458.9	49,070.2	31,972.9	12,095.6
	r/%	33.3	35.2	22.9	8.7
SLA-PECVD/NaOH-10d	Eb/eV	529.6	530.3	531.7	–
	area	53,142.9	48,769.3	17,718.9	–
	r/%	44.42	40.77	14.81	–

As shown in Table 4, the C1s XPS spectra of the SLA-PECVD/NaOH-10d sample were divided into two components with binding energies of 284.68 and 288.31 eV, which were ascribed to C–H and COO/C=O. C mainly existed in the form of C–H, with a ratio as high as 98.2%, which is why the content of C on the surface of the samples was relatively high. These results suggest that the Ti sample more easily adsorbed the organic components in the air after several days of alkali storage [28], which is also the reason why the CA of Ti sample rose faster than that of plasma oxidation.

Table 4. Binding energy, area, and proportion of the C1s peaks for the SLA-PECVD and SLA-PECVD/NaOH-10d samples.

Method	SLA-PECVD		SLA-PECVD/NaOH-10d	
	C–H	C=O	C–H	C=O
Eb/eV	284.65	289.01	284.68	288.31
area	59,223.7	4907.5	57,695.6	1056.3
r/%	92.35	7.65	98.20	1.80

In order to further analyze the changes in Ti ions at the valence bonds and the content in the deeper oxide layer, an XPS sputtering analysis of TiO_x surface was carried out. It can be seen from Figure 4 that the ratio of TiO_x content began to increase when the thickness was 40 nm. The contents of TiO_x and Ti were both almost 50 nm, which indicated that the thickness of the oxide coating was about 50 nm. However, at room temperature, the thickness range of Ti film formed in the air was in the range of 5.5–5.7 nm [28].

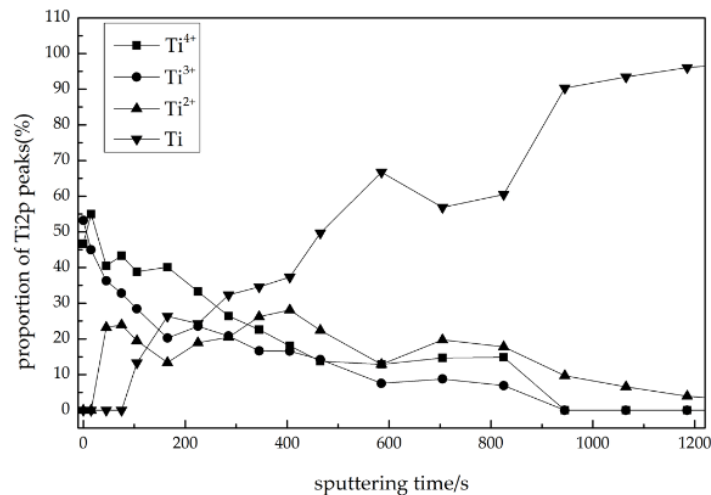


Figure 4. XPS sputtering analysis of TiO_x surface to further analyze the change of Ti ions at the valence bonds and the content in the deeper oxide layer. The contents of TiO_x and Ti were both almost 50% at 50 nm, which indicated that the thickness of the oxide coating was about 50 nm.

The XRD patterns of SLA-PECVD and SLA-PECVD/NaOH-10d are shown in Figure 5. The diffraction peak of TiO_x was not detected on the surface of Ti samples by acid etching and plasma oxidation, but the intensity of the diffraction peak of Ti changed. It was also found that the diffraction peak intensity of Ti on the surface of the sample decreased at 2θ at 35.1° , 40.2° , and 63.0° , and increased slightly at 38.4° after alkali solution treatment. The reasons for these changes need to be studied further.

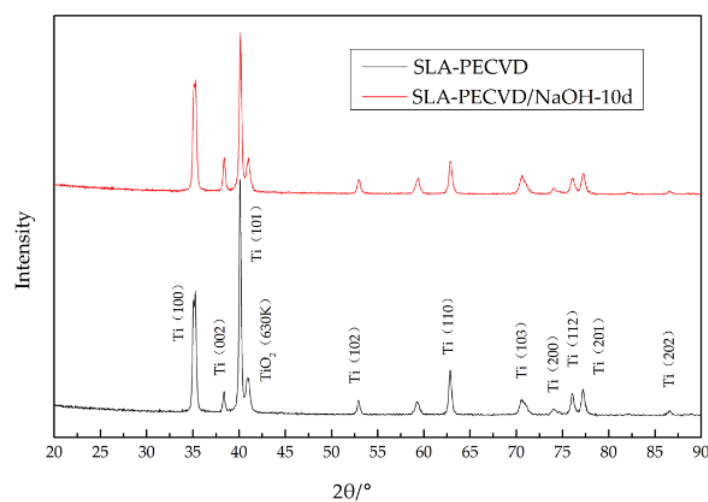


Figure 5. The XRD patterns of SLA-PECVD and SLA-PECVD/NaOH-10d samples. The diffraction peak of TiO_x was not detected on the surface of Ti samples by acid etching and plasma oxidation, but the intensity of the diffraction peak of Ti changed.

The contact angles for H₂O were 64.3 ± 3.9 , 7.88 ± 1.7 , 45.9 ± 2.9 , and 3.1 ± 0.2 degrees on the SLA, SLA/NaOH-10s, SLA-PECVD/NaOH-10s, and SLA-PECVD/NaOH-10d surfaces, respectively, indicating the super-hydrophilic status in the SLA-PECVD/NaOH-10d group (contact angle $< 5^\circ$) (Figure 6).

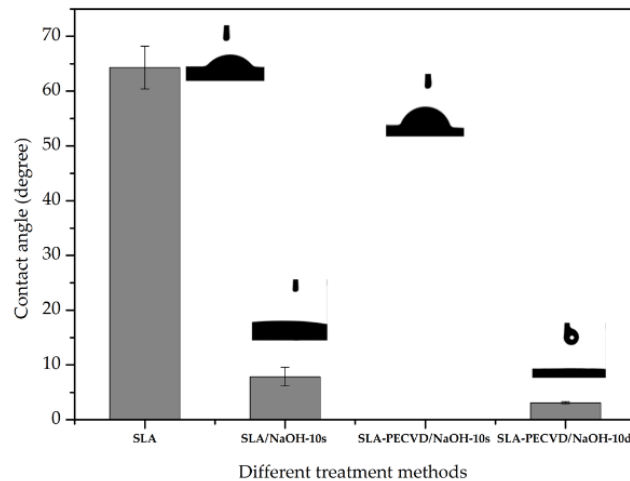


Figure 6. The contact angles for H₂O on the SLA, SLA/NaOH-10s, SLA-PECVD/NaOH-10s, and SLA-PECVD/NaOH-10d surfaces. The SLA-PECVD/NaOH-10d sample appeared to have a super-hydrophilic status.

3.2. Protein Adsorption Capacities of Ti Discs

The results of protein adsorption capacities for BSA and Fn are shown in Figure 7. After 3, 6, and 24 h of culture, the protein adsorption rates on the surface of the four groups all increased over time. ANOVA showed that at each time point, the protein adsorption rates of the four groups from high to low were SLA-PECVD/NaOH-10d > SLA-PECVD/NaOH-10s > SLA/NaOH-10s > SLA. The protein adsorption capacity of BSA for the SLA/NaOH-10s group (8.902 ± 0.435) was higher than that observed in the SLA group (5.401 ± 0.282) after 3 h incubation ($p < 0.05$). It deserves to be mentioned that the value for SLA/NaOH-10s (12.803 ± 0.565) was less than that for SLA-PECVD/NaOH-10s (17.252 ± 1.202) at 24 h, although SLA/NaOH-10s was more hydrophilic than SLA-PECVD/NaOH-10s. No significant differences were observed in the protein adhesion capacity (BSA) of SLA-PECVD/NaOH-10s samples and SLA-PECVD/NaOH-10d samples. However, the rates of Fn adsorption to Ti were significantly different among the groups ($p < 0.05$). The results of BCA show that plasma oxidation and NaOH treatment promote the adsorption of protein.

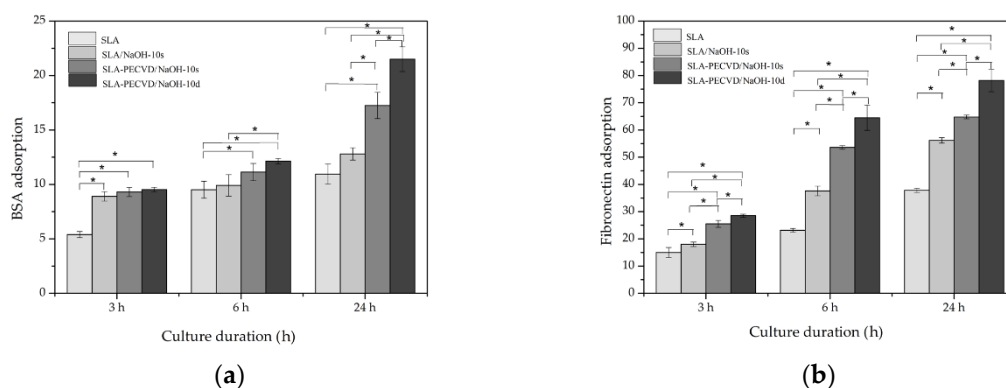


Figure 7. The results of protein adsorption capacities for bovine serum albumin (BSA) (a) and human fibronectin (Fn) (b). *: $p < 0.05$, indicating a statistically significant difference among the groups.

3.3. Cell Adhesion Capacities of Ti Discs

After 6 h of culture, the filopodium structures of osteoblasts were observed on the Ti surfaces of three groups—SLA-PECVD/NaOH-10d, SLA-PECVD/NaOH-10s, and SLA/NaOH-10s—by SEM at 5000 \times and 10,000 \times (Figure 8). Moreover, the pseudopodium of the SLA-PECVD/NaOH-10d group was longer than that of the other groups, but osteoblasts of SLA group of osteoblasts had not been observed in SLA group, and there was no such structure. As shown in Figure 8, after 24 h of cell culture, we observed that the filopodium had grown to lamellipodium on the surfaces of the SLA-PECVD/NaOH-10d, SLA-PECVD/NaOH-10s, and SLA/NaOH-10s groups, while the filamentous structure had just appeared on the SLA group. Forty-eight hours later (Figure 8), osteoblasts were lamellae structure in the groups of SLA-PECVD/NaOH-10s, SLA/NaOH-10s, and SLA, while in the SLA-PECVD/NaOH-10d group, cells completely adhered to the surface of Ti discs. Osteoblasts were observed (SEM at 50,000 \times) to stretch out and protrude into the gap of the Ti surface to form an anchor structure which adhered firmly to the surface of Ti discs.

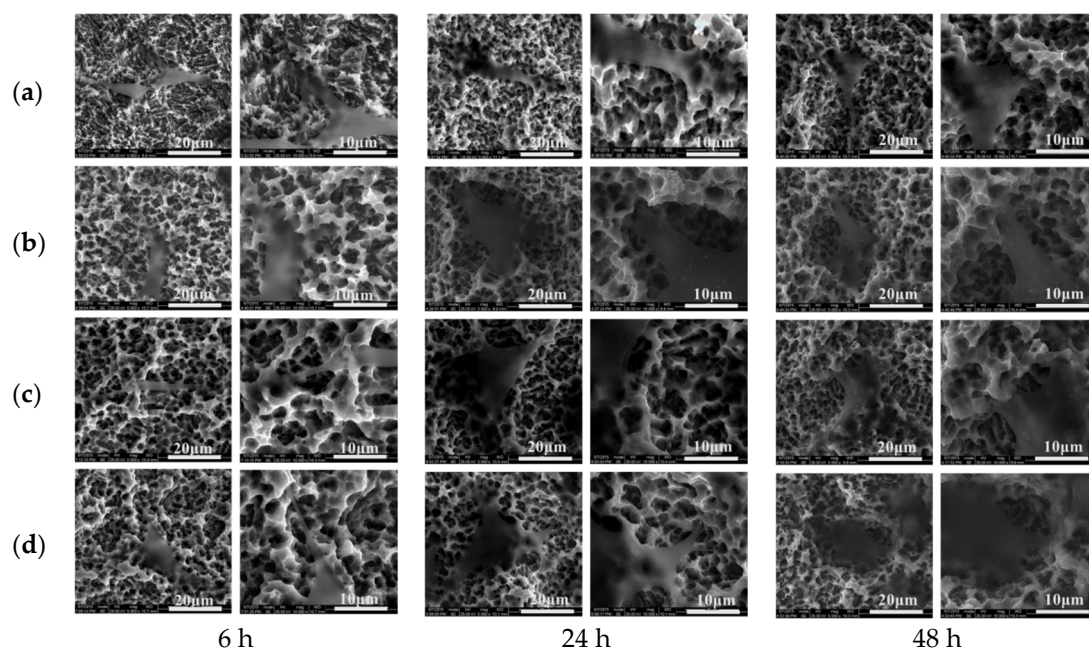


Figure 8. The structures of osteoblasts on the Ti surfaces of four groups as measured by SEM at 5000 \times and 10,000 \times after 6, 24, and 48 h of culture: (a) SLA sample; (b) SLA/NaOH-10s sample; (c) SLA-PECVD/NaOH-10s sample; and (d) SLA-PECVD/NaOH-10d sample.

3.4. Proliferation and Differentiation of Osteoblasts on Ti Discs

The MTT results of each group varied over time, as shown in Figure 9a. After 1, 3, 5, and 7 days of cell culture, the number of osteoblasts of the four groups all increased gradually over time. At the fourth time point, the order of cell proliferation from high to low was SLA-PECVD/NaOH-10d > SLA-PECVD/NaOH-10s > SLA/NaOH-10s > SLA. Moreover, the proliferation of osteoblasts was relatively slow at 1, 3, and 5 days. On the seventh day, the cells on the surfaces of the four groups significantly increased. The MTT values for the samples of the SLA/NaOH-10s group (0.270 ± 0.001) were higher than those observed for the SLA group (0.231 ± 0.020) after 7 days of incubation ($p < 0.05$). The values of the SLA-PECVD/NaOH-10d group were higher than those of the SLA-PECVD/NaOH-10s group at 1 and 5 days after seeding ($p < 0.05$). Interestingly, the MTT values of SLA/NaOH-10s (0.100 ± 0.003) were less than those of SLA-PECVD/NaOH-10s (0.115 ± 0.011) on the fifth day, although SLA/NaOH-10s samples were more hydrophilic than SLA-PECVD/NaOH-10s samples.

Total ALP activity was measured after 3, 5, 10, and 15 days of culture, as shown in Figure 9b. The ALP activity of osteoblasts on the surface of the four groups all increased with a slow and uniform

trend. The sequence was consistent with the MTT results. The ALP values in cell differentiation less in SLA than in SLA/NaOH-10s at four detection points ($p < 0.05$). The values of SLA-PECVD/NaOH-10d were higher than those of SLA-PECVD/NaOH-10s, the values of and SLA-PECVD/NaOH-10s were higher than those of SLA/NaOH-10s at 3, 5, and 15 days, respectively ($p < 0.05$).

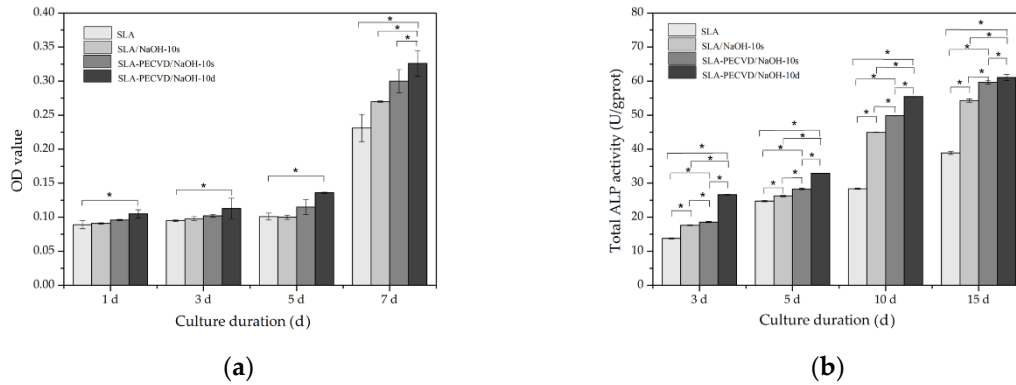


Figure 9. The MTT: (a) results and total alkaline phosphatase (ALP) and (b) activity of four groups. * $p < 0.05$, indicating a statistically significant difference among the groups.

3.5. Morphological Observation of Cytoskeleton

The images were taken by fluorescence microscope under a 20× field of vision, as shown in Figure 10. After 1 h of incubation, we observed larger MC3T3-E1 cells with extended actin filaments that were spindle-shaped on the SLA-PECVD/NaOH-10d and SLA-PECVD/NaOH-10s Ti discs, while on the SLA/NaOH-10s and SLA titanium surface, actin filaments of the cells were more circular. Among them, the spreading area of osteoblasts on the surface of SLA-PECVD/NaOH-10d group was larger than that of the other three groups, and almost all cells were spread out. After 4 h of culture, the spreading cell area of the four groups increased significantly, and the order of the spreading area was SLA-PECVD/NaOH-10d > SLA-PECVD/NaOH-10s > SLA/NaOH-10s > SLA. All the cells in the field of vision were enlarged and the extension length was evidently increased, and there was no significant difference in the shape and size of cells among the Ti discs from different groups at 24 h after seeding.

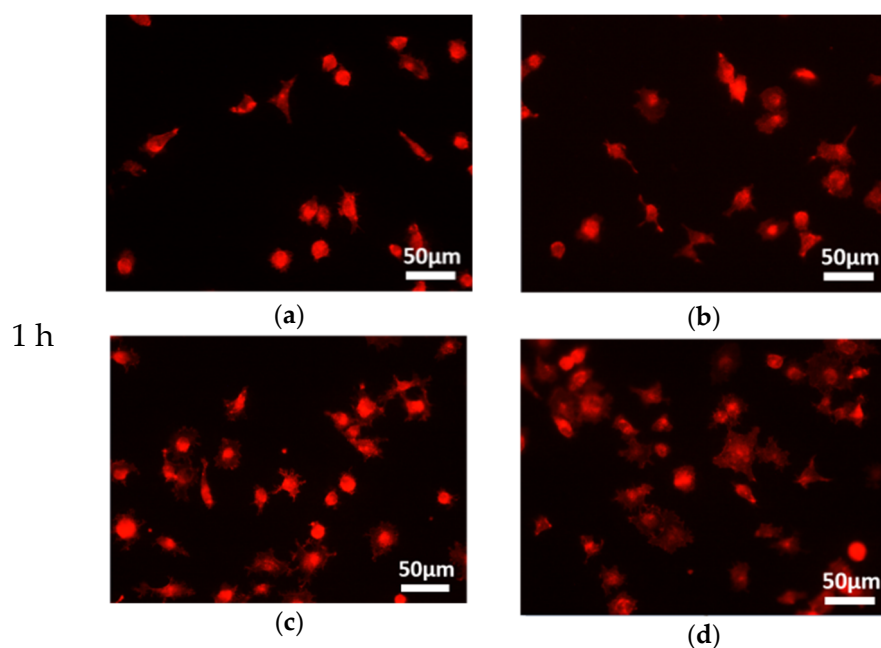


Figure 10. Cont.

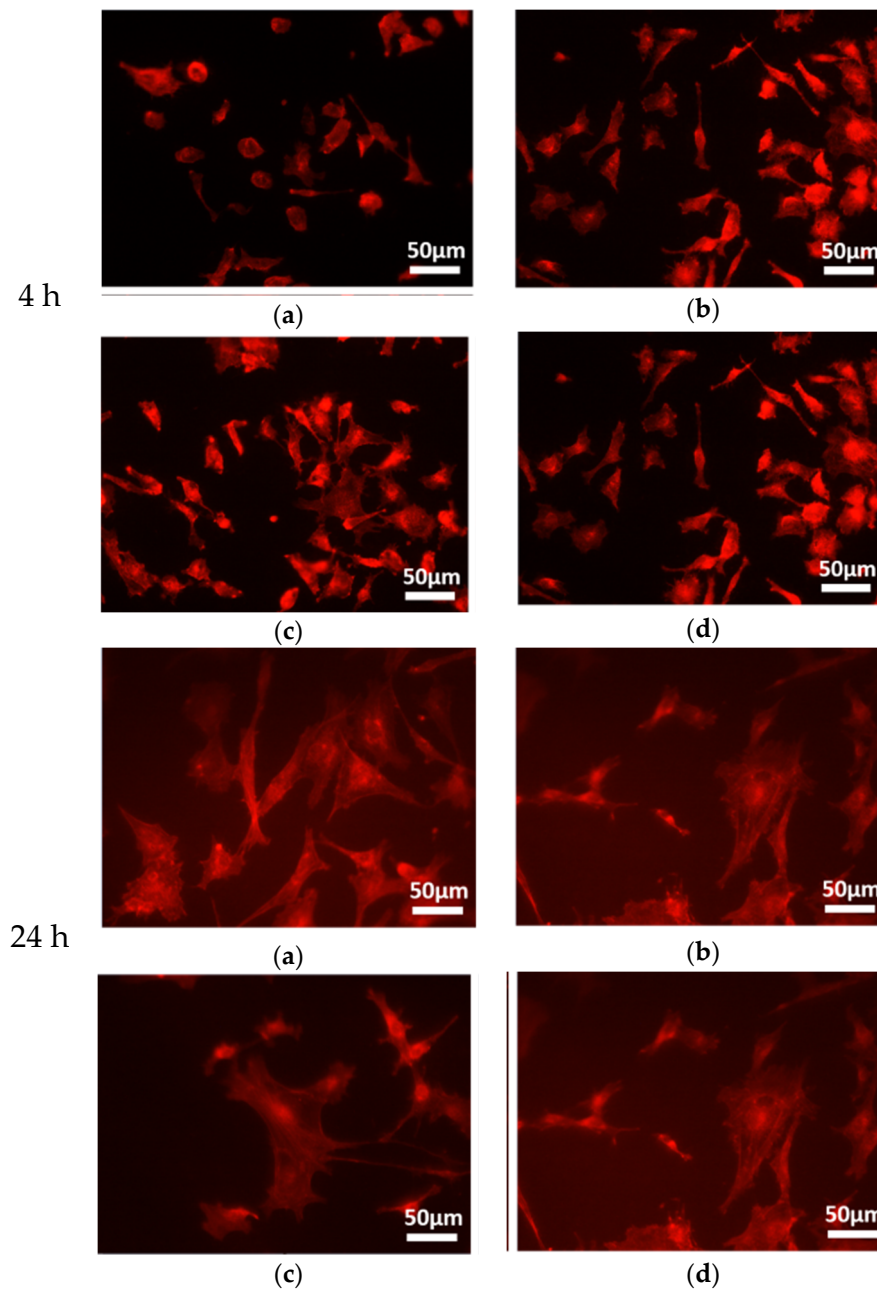


Figure 10. The images of fluorescence microscope under a 20× field of vision at 1, 4, and 24 h of incubation: (a) SLA sample; (b) SLA/NaOH-10s sample; (c) SLA-PECVD/NaOH-10s sample; and (d) SLA-PECVD/NaOH-10d sample.

4. Discussion

It has been demonstrated that implant surfaces with micro-and/or nanostructures are associated with increased production of cell adhesion molecules, bone-related extracellular matrix proteins, and distinct cellular signals, which may benefit the bioactivity and osseointegration of the implants [4,14,15,18,29–31]. At the micro-and/or nanostructure level, Jaw's hierarchical structure is imitated in terms of surface modification by the implants, which are available in the clinical setting [32]. In both short-term osseointegration of implants and long-term clinical application, the surface roughness, chemistry, and hydrophilicity of the implants play important roles. Previous research has shown that Ti surface hydrophilicity increases, the adsorption of fibronectin in the extracellular matrix (ECM) is facilitated, and cell adhesion and proliferation accelerate, including in

osteoblastic cells [33–36]. PECVD treatment can improve the surface hydrophilicity of materials [37], but the effect cannot be maintained for a long time as there is no special reserve on the surface of TiO_x film, which makes it easy for materials to adsorb hydrocarbons in the air and become hydrophobic. Thus, it is necessary to find an effective preservative. A study has shown that sodium titanate and rutile can be formed on the surface of Ti through soaking in NaOH solution, which determines the bioactivity of the surface [38]. However, the effects of this bioactive surface layer on the activity of osteoblasts and their mechanisms are still unclear. The objective of this study was to evaluate the effect of NaOH treatment on the maintenance and restoration of the surface hydrophilicity of Ti discs, and the relationship between the changes in hydrophilic properties on the titanium surfaces and the biological properties. The CA analysis indicated that the SLA-PECVD/NaOH-10d group has a super-hydrophilic status. No morphological changes were found on the super-hydrophilic surfaces of Ti discs. Under in vitro conditions, osteoblasts cultured on Ti discs showed a sequence of biological events as follows: cell adhesion, proliferation, differentiation, and mineralization [23]. Our investigation showed that super-hydrophilic surfaces were superior to other groups in these respects. The results tell us that, in terms of shelf storage, NaOH storage has an effect on the biological aging of dental implants.

The surface modification of materials can be divided into physical, chemical, and combinations of physicochemical methods. Physical modification mainly changes the micro-morphology of the implant surface through processes such as sandblasting and acid etching. Chemical modification mainly changes the chemical composition of the implant surface in order to facilitate the adsorption of cells and biologically active macromolecules around implants through processes such as anodic plasma oxidation, dispersed deposition of calcium phosphate crystals, and sputtering coating and plasma oxidation [39–41]. Since smooth implants are inferior to their microrough counterparts, the biological response of bone is influenced by the surface topography of the implants [42]. The PECVD technique used in this study is a simple, controllable, and cost-effective way to prepare a predictable coating with micrometer structure, large thickness, high hardness, and superior wear resistance. SLA surface treatment is one of the most widely used methods in the field of implant surface modification [43,44]. A series of papers confirmed that the submicron and nanostructures of SLA increase the adhesion and proliferation of cells and the percentage of bone–implant contact [45–47]. In the present study, a physicochemical method (SLA-PECVD) was used, which prepared hydrophilic surfaces that promoted the adhesion and proliferation of osteoblast [48]. Therefore, the microstructure of Ti surface should not be changed by PECVD. In this paper, there were no obvious differences in the surface morphologies of the four groups of Ti discs, which indicated that they all had optimized scaffolds. However, there was no special reserve on the surface of TiO_x film, which made it easy for materials to adsorb hydrocarbons in the air and become hydrophobic. This result is consistent with that shown for N_2 plasma by Matsubara [49].

Among the many surface modifications of Ti implants, such as sandblasting, acid etching, oxidizing, or combinations of these techniques, more attention has been paid to the increase of surface hydrophilicity [50]. In recent years, the biological effect of the hydrophilic surfaces of Ti materials on osteoblasts has been gradually recognized by researchers. However, less is known about the intrinsic wettability of bone and how best to mimic such a property. In the present study, the hydrophilicity of the material was maintained and restored in different ways, and the hydrophilicity was found to have the order $SLA < SLA/NaOH-10s < SLA-PECVD/NaOH-10s < SLA-PECVD/NaOH-10d$, indicating a super-hydrophilic status for the SLA-PECVD/NaOH-10d group. However, the comparison of hydrophilicity between the same materials with the same processing technology showed the order $SLA-PECVD/NaOH-10d > SLA-PECVD/NaOH-10s$, $SLA/NaOH-10s > SLA$. The implant surface interacted with bioactivators, and then through the binding of the active recognition sites between the cell and the factors, the interaction information between the material and the cell was transferred into the cell, thus regulating the expression of related genes [51]. Protein adsorption directly affects the adhesion, proliferation, and differentiation of osteoblasts, so the ability of a material to adsorb proteins

could reflect its biological activity. Albumin plays an important role in transporting biomolecules with low water solubility (including lipophilic molecules and calcium ions) to regulate the blood volume. Albumin lipid regulates the amplitude of intracellular calcium ions, stimulates the proliferation of osteoblasts [52], and enhances the fibronectin–integrin interaction [53]. Fn is an important extracellular matrix protein, which can promote cell adhesion and expansion. It has been shown that the higher the hydrophilicity of the material is, the stronger its ability to promote protein adsorption is [7,54]. In this experiment, the rates of Fn adsorption to Ti were significantly different among these groups ($p < 0.05$). The protein adsorption capacity of BSA for the SLA/NaOH-10s group (8.902 ± 0.435) was higher than that observed for the SLA group (5.401 ± 0.282) after 3 h of incubation ($p < 0.05$). It was interesting that the values of the SLA/NaOH-10s group (12.803 ± 0.565) were less than those of the SLA-PECVD/NaOH-10s group (17.252 ± 1.202) at 24 h, although the SLA/NaOH-10s group was shown to be more hydrophilic than the SLA-PECVD/NaOH-10s group. It is likely that the TiO_x film can affect protein adsorption, but further investigation is needed to verify this assumption. In addition, the mechanism of how the hydrophilic properties of the Ti surface affect protein adsorption needs to be studied further.

Studies have shown that, compared with hydrophobic surfaces, the proliferation, differentiation, osteoblast adhesion, and bone mineralization of hydrophilic surfaces can be significantly improved in the early stages [44,55]. Under in vitro conditions, the expression levels of ALP and the osteogenic differentiation products OCN and OPN were significantly higher on the surface of super-hydrophilic SLA than on SLA, and the levels of TGF- β 1 and PGE2, which are related to osteogenesis, were also higher than those on the surface of SLA [56]. According to the SEM images, the filopodium structures of osteoblasts were observed on the Ti surfaces of the SLA-PECVD/NaOH-10d, SLA-PECVD/NaOH-10s, and SLA/NaOH-10s groups. Moreover, the pseudopodium of the cells cultivated on the SLA-PECVD/NaOH-10d group samples was longer than that of the other groups, but the osteoblasts of the SLA group exhibited a stretching morphology, and there was no such structure at 6 h after seeding. It is well known that cells must adhere to the surface of the material before they can migrate, differentiate, and proliferate further. MTT is a sensitive and convenient method for determining the number of living cells. So, MTT values increase with an increase in cell attachment. The MTT values for the SLA/NaOH-10s group (0.270 ± 0.001) were higher than those observed for the SLA group (0.231 ± 0.020) after 7 days of incubation ($p < 0.05$). Similarly, the values of the SLA-PECVD/NaOH-10d were higher than those of the SLA-PECVD/NaOH-10s group at 1 and 5 days after seeding ($p < 0.05$). It deserves to be mentioned that the MTT values of SLA/NaOH-10s (0.100 ± 0.003) were less than those of the SLA-PECVD/NaOH-10s group (0.115 ± 0.011) on the fifth day, although SLA/NaOH-10s samples were shown to be more hydrophilic than SLA-PECVD/NaOH-10s samples. ALP values in cell differentiation were lower in SLA than in SLA/NaOH-10s at four detection points ($p < 0.05$). The values of SLA-PECVD/NaOH-10d were higher than for SLA-PECVD/NaOH-10s and the values of SLA-PECVD/NaOH-10s were higher than those of SLA/NaOH-10s at 3, 5, and 15 days, respectively ($p < 0.05$). The above results show that the better hydrophilicity of the materials prepared by a given technology, the higher the corresponding biological properties are. Hydrophilic surfaces were shown to promote the adhesion, proliferation, and differentiation of osteoblasts on the surface of Ti discs, and the results are the same as those in the previous study [25]. It is worth pointing out that for the SLA/NaOH-10s and SLA-PECVD/NaOH-10s groups, the MTT values of SLA/NaOH-10s were less than those of SLA-PECVD/NaOH-10s, although SLA/NaOH-10s were more hydrophilic than SLA-PECVD/NaOH-10s. This difference is likely due to the oxidation film having a certain effect on the biological properties and this requires further investigation.

Several studies have found that the inevitable storage of Ti implants in sterile, gas-permeable packaging during commercial distribution can result in substantially reduced protein adsorption capacity, chemotaxis-like remote attracting and adhering capabilities for osteoblasts, and changes in other bioactivity parameters relevant to osteoblast function, regardless of the surface topography [57,58]. The approaches used in this study enhanced the hydrophilicity of implants through producing clean

surfaces. However, Hashimoto et al. [59] reported that clean surfaces are in a metastable state, and thus, a completely clean surface cannot be obtained, because ambient conditions will easily cause re-contamination. This is because some organic impurities can contaminate the Ti implant surface during shelf storage, for example hydrocarbons and polycarbonyls [17,60,61]. Hayashi R et al. [62] reported that the amount of surface carbon is inversely proportional to the surface hydrophilicity, which is not unfavorable for osteoblast activity. However, in this study, the presence of C on the surface of Ti discs after soaking in NaOH solution mainly existed in the C–H form, with a ratio of as high as 98.2%. This could be due to the exposure of the Ti⁴⁺ sites, as these exposed cationic sites can contribute to the increase in the hydrophilicity and promote interactions between the proteins and cells [24]. According to the report by Xiong L B et al. [63], Ti³⁺ surface defects (TSD) represent one of the most important surface defects in TiO₂. Just like the results of this study, the content of Ti⁴⁺ increased from 46.74% to 52.09%.

It has been reported that, in a group clinical case, hydrophobic BAE surfaces were hydrophilized by alkali treatment [64], and the result was that the implants gained a good implant stability quotient (ISQ) and vertical bone volume up to one year after loading. In this study, the SLA-PECVD/NaOH-10d group was stored in NaOH liquid directly after being made in a vacuum chamber. The samples had not been exposed to air from beginning to end, and their surfaces were super-hydrophilic. However, the SLA-PECVD/NaOH-10s group was stored in the air directly, even when they were treated with NaOH liquid for a short time, so the super-hydrophilic state could not be restored. It is concluded that the hydrophilicity of Ti discs can be maintained by storage in NaOH solution. The results also showed that the hydrophilicity of SLA/NaOH-10s group was significantly higher than that of the SLA group, suggesting that NaOH liquid has a positive effect on the maintenance and restoration of hydrophilicity on the surface of pure Ti.

5. Conclusions

In this in vitro study, the results of the CA test showed that the superhydrophilicity of Ti surfaces can be effectively maintained by long-term storage in 0.1 mol/L NaOH solution. However, the surface hydrophilicity of Ti discs exposed to air can be restored to a certain extent by NaOH solution, but the superhydrophilic state cannot be restored. Combined with the SEM results of the four groups, this indicated that the surface morphology of Ti discs did not change in the process. Our results showed that the hydrophilicity of samples prepared by the same technology could enhance the protein adsorption capacity and the ability to adhere, proliferate, differentiate, and spread osteoblasts. Our findings also suggest that hydrophilicity on the surface of the materials is beneficial to the biological activity of osteoblasts. Because the Ti samples used in our study were small round discs, the results of this study may not be applicable to a structurally complex dental implant. Therefore, further in vivo experiments are warranted to investigate whether these in vitro results are applicable in clinical settings to ensure the long-term survival or possibility of early loading of dental implants.

Author Contributions: Conceptualization, L.J.; Data Curation, S.J.; Formal Analysis, S.G.; Funding Acquisition, Z.L. and B.Z.; Investigation, S.J.; Project Administration, L.J.; Resources, C.D.; Supervision, Z.L. and B.Z.; Validation, S.G.; Visualization, L.J.; Writing—Original Draft, L.J.; Writing—Review and Editing, Z.L. and B.Z.

Funding: This research was funded by the National Natural Science Foundation of China (No.51775096) and the Nature Sciences Foundation of Liaoning Province of China (Nos. 20170541059, 2013225049).

Acknowledgments: The authors would like to thank Zeng Lin research team of Department, School of Mechanical Engineering & Automation, Northeastern University for supplying the experiments instruments and Ti discs.

Conflicts of Interest: The authors declare no conflict of interest.

References

1. Ekelund, J.A.; Lindquist, L.W.; Carlsson, G.E.; Jemt, T. Implant treatment in the edentulous mandible: A prospective study on Branemark system implants over more than 20 years. *Int. J. Prosthodont.* **2003**, *16*, 602–608. [[PubMed](#)]

2. Xiao, J.R.; Kong, L.; Chen, Y.X.; Han, X.X.; Li, Y.F. Selection of optimal expansion angle and length of an expandable implant in the osteoporotic mandible: A three-dimensional finite element analysis. *Int. J. Oral Maxillofac. Implants* **2013**, *28*, e88–e97. [[CrossRef](#)]
3. Weinlaender, M.; Kenney, E.B.; Lekovic, V.; Beumer, J., 3rd; Moy, P.K.; Lewis, S. Histomorphometry of bone apposition around three types of endosseous dental implants. *Int. J. Oral Maxillofac. Implants* **1992**, *7*, 491–496.
4. Ogawa, T.; Nishimura, I. Different bone integration profiles of turned and acid-etched implants associated with modulated expression of extracellular matrix genes. *Int. J. Oral Maxillofac. Implants* **2003**, *18*, 200–210. [[PubMed](#)]
5. Att, W.; Tsukimura, N.; Suzuki, T.; Ogawa, T. Effect of supramicron roughness characteristics produced by 1- and 2-step acid etching on the osseointegration capability of titanium. *Int. J. Oral Maxillofac. Implants* **2007**, *22*, 719–728.
6. Khang, D.; Lu, J.; Yao, C.; Haberstroh, K.M.; Webster, T.J. The role of nanometer and sub-micron surface features on vascular and bone cell adhesion on titanium. *Biomaterials* **2008**, *29*, 970–983. [[CrossRef](#)]
7. Att, W.; Ogawa, T. Biological aging of implant surfaces and their restoration with ultraviolet light treatment: A novel understanding of osseointegration. *Int. J. Oral Maxillofac. Implants* **2012**, *27*, 753–761. [[PubMed](#)]
8. Najeeb, S.; Bds, Z.K.; Bds, S.Z.; Bds, M.S. Bioactivity and Osseointegration of PEEK Are Inferior to Those of Titanium: A Systematic Review. *J. Oral Implantol.* **2016**, *42*, 512–516. [[CrossRef](#)]
9. Le Guehennec, L.; Soueidan, A.; Layrolle, P.; Amouriq, Y. Surface treatments of titanium dental implants for rapid osseointegration. *Dent. Mater.* **2007**, *23*, 844–854. [[CrossRef](#)]
10. Marenzi, G.; Impero, F.; Scherillo, F.; Sammartino, J.C.; Squillace, A.; Spagnuolo, G. Effect of Different Surface Treatments on Titanium Dental Implant Micro-Morphology. *Materials* **2019**, *12*, 733. [[CrossRef](#)]
11. Janson, O.; Gururaj, S.; Pujari-Palmer, S.; Karlsson Ott, M.; Stromme, M.; Engqvist, H.; Welch, K. Titanium surface modification to enhance antibacterial and bioactive properties while retaining biocompatibility. *Mater. Sci. Eng. C Mater. Biol. Appl.* **2019**, *96*, 272–279. [[CrossRef](#)] [[PubMed](#)]
12. Rupp, F.; Scheideler, L.; Rehbein, D.; Axmann, D.; Geis-Gerstorfer, J. Roughness induced dynamic changes of wettability of acid etched titanium implant modifications. *Biomaterials* **2004**, *25*, 1429–1438. [[CrossRef](#)]
13. Gittens, R.A.; Olivares-Navarrete, R.; Cheng, A.; Anderson, D.M.; McLachlan, T.; Stephan, I.; Geis-Gerstorfer, J.; Sandhage, K.H.; Fedorov, A.G.; Rupp, F.; et al. The roles of titanium surface micro/nanotopography and wettability on the differential response of human osteoblast lineage cells. *Acta Biomater.* **2013**, *9*, 6268–6277. [[CrossRef](#)]
14. Att, W.; Hori, N.; Takeuchi, M.; Ouyang, J.; Yang, Y.; Anpo, M.; Ogawa, T. Time-dependent degradation of titanium osteoconductivity: An implication of biological aging of implant materials. *Biomaterials* **2009**, *30*, 5352–5363. [[CrossRef](#)]
15. Hori, N.; Att, W.; Ueno, T.; Sato, N.; Yamada, M.; Saruwatari, L.; Suzuki, T.; Ogawa, T. Age-dependent degradation of the protein adsorption capacity of titanium. *J. Dent. Res.* **2009**, *88*, 663–667. [[CrossRef](#)]
16. Kilpadi, D.V.; Lemons, J.E.; Liu, J.; Raikar, G.N.; Weimer, J.J.; Vohra, Y. Cleaning and heat-treatment effects on unalloyed titanium implant surfaces. *Int. J. Oral Maxillofac. Implants* **2000**, *15*, 219–230. [[PubMed](#)]
17. Serro, A.P.; Saramago, B. Influence of sterilization on the mineralization of titanium implants induced by incubation in various biological model fluids. *Biomaterials* **2003**, *24*, 4749–4760. [[CrossRef](#)]
18. Lu, H.; Wan, L.; Zhang, X.; Rong, M.; Guo, Z.; Zhou, L. Effects of Hydrocarbons Contamination on Initial Responses of Osteoblast-like Cells on Acid-Etched Titanium Surface. *Rare Met. Mater. Eng.* **2013**, *42*, 1558–1562.
19. Tugulu, S.; Lowe, K.; Scharnweber, D.; Schlottig, F. Preparation of superhydrophilic microrough titanium implant surfaces by alkali treatment. *J. Mater. Sci. Mater. Med.* **2010**, *21*, 2751–2763. [[CrossRef](#)] [[PubMed](#)]
20. Sakai, N.; Wang, R.; Fujishima, A.; Watanabe, T.; Hashimoto, K. Effect of ultrasonic treatment on highly hydrophilic TiO₂ surfaces. *Langmuir* **1998**, *14*, 5918–5920. [[CrossRef](#)]
21. Connor, P.A.; Dobson, K.D.; Mcquillan, A.J. Infrared spectroscopy of the TiO₂/aqueous solution interface. *Langmuir* **1999**, *15*, 2402–2408. [[CrossRef](#)]
22. Gembitsky, D.S.; Lawlor, K.; Jacovina, A.; Yaneva, M.; Tempst, P. A prototype antibody microarray platform to monitor changes in protein tyrosine phosphorylation. *Mol. Cell. Proteom.* **2004**, *3*, 1102–1118. [[CrossRef](#)]
23. Aita, H.; Hori, N.; Takeuchi, M.; Suzuki, T.; Yamada, M.; Anpo, M.; Ogawa, T. The effect of ultraviolet functionalization of titanium on integration with bone. *Biomaterials* **2009**, *30*, 1015–1025. [[CrossRef](#)] [[PubMed](#)]

24. Choi, S.H.; Jeong, W.S.; Cha, J.Y.; Lee, J.H.; Yu, H.S.; Choi, E.H.; Kim, K.M.; Hwang, C.J. Time-dependent effects of ultraviolet and nonthermal atmospheric pressure plasma on the biological activity of titanium. *Sci. Rep.* **2016**, *6*, 33421. [[CrossRef](#)] [[PubMed](#)]
25. Seo, H.Y.; Kwon, J.S.; Choi, Y.R.; Kim, K.M.; Choi, E.H.; Kim, K.N. Cellular attachment and differentiation on titania nanotubes exposed to air- or nitrogen-based non-thermal atmospheric pressure plasma. *PLoS ONE* **2014**, *9*, e113477. [[CrossRef](#)]
26. Wu, J.; Zhou, L.; Ding, X.; Gao, Y.; Liu, X. Biological Effect of Ultraviolet Photocatalysis on Nanoscale Titanium with a Focus on Physicochemical Mechanism. *Langmuir* **2015**, *31*, 10037–10046. [[CrossRef](#)]
27. Canullo, L.; Genova, T.; Tallarico, M.; Gautier, G.; Mussano, F.; Botticelli, D. Plasma of Argon Affects the Earliest Biological Response of Different Implant Surfaces: An In Vitro Comparative Study. *J. Dent. Res.* **2016**, *95*, 566–573. [[CrossRef](#)]
28. Massaro, C.; Rotolo, P.; De Riccardis, F.; Milella, E.; Napoli, A.; Wieland, M.; Textor, M.; Spencer, N.D.; Brunette, D.M. Comparative investigation of the surface properties of commercial titanium dental implants. Part I: Chemical composition. *J. Mater. Sci. Mater. Med.* **2002**, *13*, 535–548. [[CrossRef](#)]
29. Nakamura, H.K.; Butz, F.; Saruwatari, L.; Ogawa, T. A role for proteoglycans in mineralized tissue-titanium adhesion. *J. Dent. Res.* **2007**, *86*, 147–152. [[CrossRef](#)] [[PubMed](#)]
30. Kubo, K.; Tsukimura, N.; Iwasa, F.; Ueno, T.; Saruwatari, L.; Aita, H.; Chiou, W.A.; Ogawa, T. Cellular behavior on TiO₂ nanonodular structures in a micro-to-nanoscale hierarchy model. *Biomaterials* **2009**, *30*, 5319–5329. [[CrossRef](#)] [[PubMed](#)]
31. Ogawa, T.; Nishimura, I. Genes differentially expressed in titanium implant healing. *J. Dent. Res.* **2006**, *85*, 566–570. [[CrossRef](#)]
32. Wennerberg, A.; Svanborg, L.M.; Berner, S.; Andersson, M. Spontaneously formed nanostructures on titanium surfaces. *Clin. Oral Implants Res.* **2013**, *24*, 203–209. [[CrossRef](#)] [[PubMed](#)]
33. Canullo, L.; Genova, T.; Wang, H.L.; Carossa, S.; Mussano, F. Plasma of Argon Increases Cell Attachment and Bacterial Decontamination on Different Implant Surfaces. *Int. J. Oral Maxillofac. Implants* **2017**, *32*, 1315–1323. [[CrossRef](#)] [[PubMed](#)]
34. Calciolari, E.; Hamlet, S.; Ivanovski, S.; Donos, N. Pro-osteogenic properties of hydrophilic and hydrophobic titanium surfaces: Crosstalk between signalling pathways in in vivo models. *J. Periodontal. Res.* **2018**, *53*, 598–609. [[CrossRef](#)] [[PubMed](#)]
35. Alves, C.M.; Yang, Y.; Carnes, D.L.; Ong, J.L.; Sylvia, V.L.; Dean, D.D.; Agrawal, C.M.; Reis, R.L. Modulating bone cells response onto starch-based biomaterials by surface plasma treatment and protein adsorption. *Biomaterials* **2007**, *28*, 307–315. [[CrossRef](#)] [[PubMed](#)]
36. Tan, F.; O'Neill, F.; Naciri, M.; Dowling, D.; Al-Rubeai, M. Cellular and transcriptomic analysis of human mesenchymal stem cell response to plasma-activated hydroxyapatite coating. *Acta Biomater.* **2012**, *8*, 1627–1638. [[CrossRef](#)]
37. Kocaman, S.; Karaman, M.; Gursoy, M.; Ahmetli, G. Chemical and plasma surface modification of lignocellulose coconut waste for the preparation of advanced biobased composite materials. *Carbohydr. Polym.* **2017**, *159*, 48–57. [[CrossRef](#)] [[PubMed](#)]
38. Yamaguchi, S.; Nath, S.; Sugawara, Y.; Divakarla, K.; Das, T.; Manos, J.; Chrzanowski, W.; Matsushita, T.; Kokubo, T. Two-in-One Biointerfaces-Antimicrobial and Bioactive Nanoporous Gallium Titanate Layers for Titanium Implants. *Nanomaterials* **2017**, *7*, 229. [[CrossRef](#)]
39. Sul, Y.T.; Johansson, C.; Byon, E.; Albrektsson, T. The bone response of oxidized bioactive and non-bioactive titanium implants. *Biomaterials* **2005**, *26*, 6720–6730. [[CrossRef](#)]
40. Mendes, V.C.; Moineddin, R.; Davies, J.E. The effect of discrete calcium phosphate nanocrystals on bone-bonding to titanium surfaces. *Biomaterials* **2007**, *28*, 4748–4755. [[CrossRef](#)]
41. Rupp, F.; Scheideler, L.; Olshanska, N.; de Wild, M.; Wieland, M.; Geis-Gerstorfer, J. Enhancing surface free energy and hydrophilicity through chemical modification of microstructured titanium implant surfaces. *J. Biomed. Mater. Res. A* **2006**, *76*, 323–334. [[CrossRef](#)]
42. Wennerberg, A.; Albrektsson, T. Effects of titanium surface topography on bone integration: A systematic review. *Clin. Oral Implants Res.* **2009**, *20*, 172–184. [[CrossRef](#)]

43. Cochran, D.L.; Buser, D.; ten Bruggenkate, C.M.; Weingart, D.; Taylor, T.M.; Bernard, J.P.; Peters, F.; Simpson, J.P. The use of reduced healing times on ITI implants with a sandblasted and acid-etched (SLA) surface: Early results from clinical trials on ITI SLA implants. *Clin. Oral Implants Res.* **2002**, *13*, 144–153. [[CrossRef](#)]
44. Bornstein, M.M.; Valderrama, P.; Jones, A.A.; Wilson, T.G.; Seibl, R.; Cochran, D.L. Bone apposition around two different sandblasted and acid-etched titanium implant surfaces: A histomorphometric study in canine mandibles. *Clin. Oral Implants Res.* **2008**, *19*, 233–241. [[CrossRef](#)]
45. Wennerberg, A.; Albrektsson, T.; Andersson, B.; Krol, J.J. A histomorphometric and removal torque study of screw-shaped titanium implants with three different surface topographies. *Clin. Oral Implants Res.* **1995**, *6*, 24–30. [[CrossRef](#)]
46. Wennerberg, A.; Hallgren, C.; Johansson, C.; Danelli, S. A histomorphometric evaluation of screw-shaped implants each prepared with two surface roughnesses. *Clin. Oral Implants Res.* **1998**, *9*, 11–19. [[CrossRef](#)]
47. Kirchhoff, H.; Borinski, M.; Lenhert, S.; Chi, L.; Buchel, C. Transversal and lateral exciton energy transfer in grana thylakoids of spinach. *Biochemistry* **2004**, *43*, 14508–14516. [[CrossRef](#)]
48. He, J.; Feng, W.; Zhao, B.H.; Zhang, W.; Lin, Z. In Vivo Effect of Titanium Implants with Porous Zinc-Containing Coatings Prepared by Plasma Electrolytic Oxidation Method on Osseointegration in Rabbits. *Int. J. Oral Maxillofac. Implants* **2018**, *33*, 298–310. [[CrossRef](#)]
49. Matsubara, K.; Danno, M.; Inoue, M.; Honda, Y.; Yoshida, N.; Abe, T. Characterization of titanium particles treated with N₂ plasma using a barrel-plasma-treatment system. *Phys. Chem. Chem. Phys.* **2013**, *15*, 5097–5107. [[CrossRef](#)]
50. Junker, R.; Dimakis, A.; Thoneick, M.; Jansen, J.A. Effects of implant surface coatings and composition on bone integration: A systematic review. *Clin. Oral Implants Res.* **2009**, *20*, 185–206. [[CrossRef](#)]
51. Hallab, N.J.; Bundy, K.J.; O'Connor, K.; Moses, R.L.; Jacobs, J.J. Evaluation of metallic and polymeric biomaterial surface energy and surface roughness characteristics for directed cell adhesion. *Tissue Eng.* **2001**, *7*, 55–71. [[CrossRef](#)]
52. Mata, A.; Su, X.; Fleischman, A.J.; Roy, S.; Banks, B.A.; Miller, S.K.; Midura, R.J. Osteoblast attachment to a textured surface in the absence of exogenous adhesion proteins. *IEEE Trans. Nanobiosci.* **2003**, *2*, 287–294. [[CrossRef](#)]
53. Pols, H.A.; Schilte, H.P.; Nijweide, P.J.; Visser, T.J.; Birkenhager, J.C. The influence of albumin on vitamin D metabolism in fetal chick osteoblast-like cells. *Biochem. Biophys. Res. Commun.* **1984**, *125*, 265–272. [[CrossRef](#)]
54. Gittens, R.A.; Scheideler, L.; Rupp, F.; Hyzy, S.L.; Geis-Gerstorfer, J.; Schwartz, Z.; Boyan, B.D. A review on the wettability of dental implant surfaces II: Biological and clinical aspects. *Acta Biomater.* **2014**, *10*, 2907–2918. [[CrossRef](#)]
55. Eriksson, C.; Nygren, H.; Ohlson, K. Implantation of hydrophilic and hydrophobic titanium discs in rat tibia: Cellular reactions on the surfaces during the first 3 weeks in bone. *Biomaterials* **2004**, *25*, 4759–4766. [[CrossRef](#)]
56. Rausch-fan, X.; Qu, Z.; Wieland, M.; Matejka, M.; Schedle, A. Differentiation and cytokine synthesis of human alveolar osteoblasts compared to osteoblast-like cells (MG63) in response to titanium surfaces. *Dent. Mater.* **2008**, *24*, 102–110. [[CrossRef](#)]
57. Ghassemi, A.; Ishijima, M.; Hasegawa, M.; Mohammadzadeh Rezaei, N.; Nakhaei, K.; Sekiya, T.; Torii, Y.; Hirota, M.; Park, W.; Miley, D.D.; et al. Biological and Physicochemical Characteristics of 2 Different Hydrophilic Surfaces Created by Saline-Storage and Ultraviolet Treatment. *Implant Dent.* **2018**, *27*, 405–414. [[CrossRef](#)]
58. Choi, S.H.; Jeong, W.S.; Cha, J.Y.; Lee, J.H.; Lee, K.J.; Yu, H.S.; Choi, E.H.; Kim, K.M.; Hwang, C.J. Effect of the ultraviolet light treatment and storage methods on the biological activity of a titanium implant surface. *Dent. Mater.* **2017**, *33*, 1426–1435. [[CrossRef](#)]
59. Hashimoto, K.; Irie, H.; Fujishima, A. TiO₂ photocatalysis: A historical overview and future prospects. *Jpn. J. Appl. Phys.* **2005**, *44*, 8269–8285.
60. Kasemo, B.; Lausmaa, J. Biomaterial and implant surfaces: On the role of cleanliness, contamination, and preparation procedures. *J. Biomed. Mater. Res.* **1988**, *22*, 145–158. [[CrossRef](#)]
61. Lee, J.H.; Ogawa, T. The biological aging of titanium implants. *Implant Dent.* **2012**, *21*, 415–421. [[CrossRef](#)]
62. Hayashi, R.; Ueno, T.; Migita, S.; Tsutsumi, Y.; Doi, H.; Ogawa, T.; Hanawa, T.; Wakabayashi, N. Hydrocarbon Deposition Attenuates Osteoblast Activity on Titanium. *J. Dent. Res.* **2014**, *93*, 698–703. [[CrossRef](#)]

63. Xiong, L.; Li, J.; Yang, B.; Yu, Y. Ti^{3+} in the Surface of Titanium Dioxide: Generation, Properties and Photocatalytic Application. *J. Nanomater.* **2012**, *2012*, 831524. [[CrossRef](#)]
64. Held, U.; Rohner, D.; Rothamel, D. Early loading of hydrophilic titanium implants inserted in low-mineralized (D3 and D4) bone: One year results of a prospective clinical trial. *Head Face Med.* **2013**, *9*, 37. [[CrossRef](#)]



© 2019 by the authors. Licensee MDPI, Basel, Switzerland. This article is an open access article distributed under the terms and conditions of the Creative Commons Attribution (CC BY) license (<http://creativecommons.org/licenses/by/4.0/>).